



Cite this: *RSC Adv.*, 2024, 14, 37737

# Application of machine learning in developing a quantitative structure–property relationship model for predicting the thermal decomposition temperature of nitrogen-rich energetic ionic salts†

Yunling Zhang,<sup>a</sup> Liang Fan,<sup>b</sup> Chao Su,<sup>c</sup> Zhenyu Shu<sup>\*d</sup> and Haijie Zhang <sup>\*b</sup>

While thermal decomposition temperature ( $T_d$ ) is one of the most important indexes for energetic materials, the most common way of determining and evaluating  $T_d$  requires laboratory experiments that are complicated, time-consuming and expensive. In the present study, the quantitative structure–property relationship (QSPR) model of  $T_d$  for 21 nitrogen-rich energetic ionic salts was built and used for  $T_d$  prediction through 13 descriptors and principal component analysis. The relatively small dataset of 21 samples may lead to overfitting. In the case of small datasets, possible overfitting was reduced by the support vector machine to derive the non-linear QSPR model. The obtained correlation coefficient ( $R^2$ ) of 96.31% and root-mean-square error (RMSE) of 15.72 indicate the relative reliability of the QSPR model developed in this work. Moreover,  $T_d$  values of 6 newly designed nitrogen-rich energetic ionic salts were predicted using the new QSPR model. The predicted  $T_d$  values range from 194 to 225 °C, which are better than that of 4-amino-3,5-dinitro-1*H*-pyrazole (LLM-116: 178 °C), and no. 1, 2 and 5 are comparable to that of the traditional explosive 1,3,5-trinitro-1,3,5-triazinane (RDX: 230 °C), indicating the excellent properties of the designed energetic ionic salts, which can be used for the preparation of potential energetic materials.

Received 13th August 2024  
Accepted 4th November 2024

DOI: 10.1039/d4ra05875e

rsc.li/rsc-advances

## 1. Introduction

Energetic materials, such as explosives, propellants, and pyrotechnics, are widely used in the civil industry and military applications. In addition to good detonation performance characterized by high detonation velocity and pressure and high heat of formation, energetic materials should exhibit good stability in order to ensure that they are stored and transported safely. Thermal stability is a particularly important property of energetic materials because the amount of energy released during the decomposition process is closely related to chemical reactivity.<sup>1</sup> The thermal stability of energetic materials can be determined using calorimetric measurements to evaluate their temperature and heat of decomposition.<sup>1,2</sup> Overall, thermal decomposition temperature ( $T_d$ ) is the most widely used

parameter to characterize the thermal stability of energetic materials.

Recently, nitrogen-rich energetic ionic salts have attracted more attention than their nonionic analogues. Unlike nonionic explosives, ionic salts are composed of cations and anions, both of which may participate in the decomposition and explosion process, possessing lower vapor pressure, higher density, and higher thermal stability.<sup>3–8</sup> Nitrogen-rich heterocyclic compounds such as furazan (furoxan) and tetrazole are currently the focus of research activities in the field of energetic ionic salts, where multiple experimental<sup>3–5</sup> and theoretical<sup>9</sup> studies have been performed. Being energetic materials, nitrogen-rich energetic ionic salts possess good thermal stability in order to decrease the risk of a catastrophic explosion.<sup>10</sup> Machine learning (ML), as a type of artificial intelligence, is a data-driven technology that uses algorithms to parse, learn, and predict data. The important advantage of ML is that once an algorithm learns how to process data, it can automatically complete the prediction work, avoiding hazardous, complicated, time-consuming and expensive experiments. Recently, ML, which is capable of overcoming the well-known shortcomings of the existing experimental methods and techniques, has attracted the attention of the wide research community working in chemistry, materials science, medicine and other related fields.<sup>11–18</sup>

<sup>a</sup>Beiyuan Campus, Beijing Vocational College of Agriculture, Beijing, 100012, China

<sup>b</sup>State Key Laboratory of Environmental Criteria and Risk Assessment, Chinese Research Academy of Environmental Sciences, Beijing 100012, China. E-mail: zhanghaijie@craes.org.cn

<sup>c</sup>Taiji Computer Co., Ltd, Beijing, 100012, China

<sup>d</sup>School of Information Science and Engineering, Ningbo Institute of Technology, Zhejiang University, Ningbo, 315100, China. E-mail: shuzhenyu@nit.zju.edu.cn

† Electronic supplementary information (ESI) available. See DOI: <https://doi.org/10.1039/d4ra05875e>


The method of establishing a correlation between physical or chemical properties of a compound and its molecular structure *via* various descriptors, such as quantitative structure–property relationship (QSPR), is particularly good at modeling and predicting the properties of new energetic materials, such as impact sensitivity,<sup>11,19–22</sup> density,<sup>12,23–25</sup> melting point,<sup>26–28</sup> decomposition enthalpy,<sup>1,2</sup> detonation velocity,<sup>29,30</sup> and decomposition temperature.<sup>31–39</sup> For example, Fathollahi *et al.* employed Artificial Neural Networks (ANN) model and multiple linear regression (MLR) to predict the  $T_d$  of cocrystals and obtained the correlation coefficient  $R^2$  of 0.9784 and 0.7438, respectively.<sup>31</sup> Wang *et al.* developed two models by MLR and SVM for the prediction of self-accelerating  $T_d$  of organic peroxides and obtained the correlation coefficient  $R^2$  of 0.727 and 0.952, respectively.<sup>32</sup> Zohari *et al.* predicted the  $T_d$  of azole-based energetic compounds *via* the MLR approach and obtained the correlation coefficient  $R^2$  of the model of 0.936.<sup>34</sup> This means that the existing models for determining  $T_d$  focus mainly on the aforementioned non-ionic molecules and that in the existing QSPR models for non-ionic molecules, most of the selected descriptors carry on limited amount of information on the chemical composition of these molecules such as the number of atoms, atomic groups and chemical bonds.<sup>33,35</sup> A significant difference between energetic ionic salts and non-ionic molecules, such as the hydrogen-bonding interactions between the cations and anions, indicates that an improved QSPR model should be developed. Also, based on the literature review of our knowledge, such QSPR studies on the  $T_d$  of energetic ionic salts are lacking. In order to improve the description of the internal structure of the energetic ionic salts, 12 quantitative descriptors along with oxygen balance of the 21 samples collected from the same research group, which are closely related to the thermal property of energetic materials, were chosen as descriptors to build the QSPR model of  $T_d$  in this study.

It is important to note that the dataset used in this study is relatively small and, hence, a suitable ML algorithm for the small dataset is needed. With the development of ML, a variety of ML algorithms such as ANN, Support Vector Machines (SVM), Random Forest, and Decision Tree became available and commonly used in the development of various material QSPR models.<sup>13–15</sup> Both ANN and MLR models have limitations when applied to nitrogen-rich energetic ionic salts. While ANN is capable of modeling nonlinear relationships, it typically requires large datasets for proper training, which may not be feasible in the case of complex energetic salts where experimental data are quite scarce. On the other hand, MLR, which is simple and easy to interpret, is often inefficient in capturing the nonlinear and multivariate dependencies of such compounds. SVM, which follows the structural risk minimization principle, offers a better balance to effectively handle small dataset and modeling nonlinear relationships, possessing a higher prediction accuracy and generalization.<sup>40–45</sup> Due to the difficulties in preparing energetic ionic salts and the limited number of samples that can be collected, SVM is the most suitable model for building the  $T_d$  QSPR of energetic ionic salts.

Moreover, to reduce the computational cost and complexity of machine learning algorithms, it is necessary to perform the descriptors data in reduced dimensions. Principal Component Analysis (PCA) and Least Absolute Shrinkage and Selection Operator (LASSO) are widely used for dimensionality reduction. PCA is an unsupervised method that does not rely on target variables (labels), which makes it suitable for extracting key features from the data in the case when no clear target variable is present. In contrast, LASSO is a supervised learning method that requires target variables for feature selection. This reliance on target variables can make LASSO prone to overfitting, especially with small sample sizes. Compared to LASSO, PCA can better mitigate overfitting. At the same time, cross validation was used for parameter selection during the training of the SVM model, which can effectively avoid overfitting. The developed QSPR model was further used to predict the  $T_d$  values of 6 theoretically designed nitrogen-rich energetic ionic salts. It is important to note that while SVM is well-suited for small sample sizes, the relatively small dataset of 21 nitrogen-rich energetic ionic salts used in this study may still impose some limitations on the model generalization to a wider range of compounds. Further work should focus on expanding the dataset to improve the robustness and reliability of the model.

## 2. Computational details

### 2.1 Quantum chemical calculations

The density functional theory (DFT) proposed by Kohn *et al.*<sup>46</sup> has been continuously developed and improved into a commonly used quantum chemistry method.<sup>47–50</sup> It replaces the wave function with electron density as the fundamental quantity being studied and uses it to describe the properties of the entire system. In this paper, quantum chemical calculations were performed with the Gaussian 09 program.<sup>51</sup> Geometric optimization and frequency calculations of the energetic ionic salts were carried out at the M06-2X/6-311++G(3df,3pd) level of theory. The ability of the highly parameterized, empirical exchange–correlation functional M06-2X to deliver excellent description of a variety of different properties and processes has been long known and is confirmed by a number of studies over the past few years.<sup>52–55</sup> The basis set used here is the largest Pople basis set, which comprises relatively low computational costs with a very good performance. Computations were carried out with the convergence criteria set at tight levels. To confirm the minimum energy structures, frequency calculations were conducted and characterized by the absence of imaginary frequencies. The detailed calculation script has been presented in the (ESI).†

Thirteen general descriptors, including oxygen balance (OB) and quantum chemical descriptors, were calculated to build a QSPR model for  $T_d$ . These quantum chemical descriptors were the energy of the highest occupied molecular orbital ( $E_{\text{HOMO}}$ ), energy of the lowest unoccupied molecular orbital ( $E_{\text{LUMO}}$ ), energy gap ( $\Delta E$ ) between the highest occupied molecular orbital and the lowest unoccupied molecular orbital, total dipole moment ( $\mu$ ), polarizability ( $\alpha$ ), nucleus-independent chemical shift (NICS) for furazan (furoxan) ring, NICS for the tetrazole



ring, available free space ( $\Delta V$ ), variance of electrostatic potential value on the van der Waals molecular surface ( $\sigma^2$ ), ionization potential ( $I$ ), electron affinity ( $A$ ), and Wiberg bond order (WBO) of the weakest chemical bond. The detailed description is as follows.

OB is an index used to measure the deficiency or excess of oxygen in a compound when all carbon is converted into carbon monoxide and all hydrogen is converted into water for the compound with the molecular formula of  $C_aH_bN_cO_d$  (without crystal water),  $OB = 1600[(d - 2a - b/2)/M_r][\%]$ , in which  $M_r$  was the relative molecular mass. An OB value of zero indicates complete oxidation during the detonation. At this point, the most energy is released.<sup>56</sup> Therefore, in addition to high density and a high heat of formation, a good oxygen balance is another important factor for designing nitrogen-rich five- or six-membered heterocycles as high-performance energetic materials.<sup>56–59</sup>

The highest occupied molecular orbital (HOMO) and lowest unoccupied molecular orbital (LUMO) are the most important orbitals in a molecule, which play prominent roles in governing chemical reactions.<sup>60,61</sup>  $E_{\text{HOMO}}$  reflects the ability of a molecule to donate electrons and  $E_{\text{LUMO}}$  reflects the ability of a molecule to accept electrons.<sup>61</sup>

$\Delta E$  is an important descriptor of energetic materials, which is obtained by calculating the difference between  $E_{\text{HOMO}}$  and  $E_{\text{LUMO}}$ , affects the kinetic stability, chemical reactivity, optical polarizability, and chemical hardness-softness of a molecule.<sup>62–64</sup> Molecules with large  $\Delta E$  values have been reported to have lower chemical reactivity.<sup>20,65</sup> In other words, a larger HOMO–LUMO gap suggests a higher stability<sup>66</sup> because a large gap is not beneficial for the transition of electrons from HOMO to LUMO.<sup>20</sup>

The polarity of a molecule is reflected by its total  $\mu$  and  $\alpha$  values. The value of  $\mu$  indicates the polarity of a polar covalent bond,<sup>67</sup> which is equal to the product of charge on the two bonded atoms and the distance between them. The total molecular dipole moment of a molecule is approximately equal to the vector sum of each bond dipole moment. Thus, the total value of  $\mu$  reflects the global polarity of a molecule. Higher total  $\mu$  and  $\alpha$  values indicate a greater possibility of electrostatic interaction with other molecules.<sup>68</sup>

The NICS index proposed by Schleyer's team in 1996 (ref. 69 and 70) is based on absolute magnetic shielding and can be used to characterize aromaticity. Its physical meaning is the negative value of the magnetic shielding value set by a person that is not at the atomic nucleus position. The larger the negative value, the stronger the magnetic field shielding, indicating a stronger aromaticity. Aromaticity is highly relevant to electron delocalization in closed circuits and will lead to lower energy (often substantially lower) and a variety of unusual chemical and physical properties.<sup>70</sup> Calculating NICS at the center of a ring describes  $\sigma$  aromaticity, while calculating the NICS out of the center of the ring describes  $\pi$  aromaticity.<sup>71,72</sup> A more negative NICS value suggests a greater aromaticity. In this study,  $\lambda_{\text{NICS}(0)\text{F}}$  and  $\lambda_{\text{NICS}(0)\text{Z}}$  are the indexes of  $\sigma$  aromaticity at the mass center of the furazan (furoxan) and tetrazole rings, respectively.  $\lambda_{\text{NICS}(1)\text{F}}$  and  $\lambda_{\text{NICS}(1)\text{Z}}$  represent the NICS values

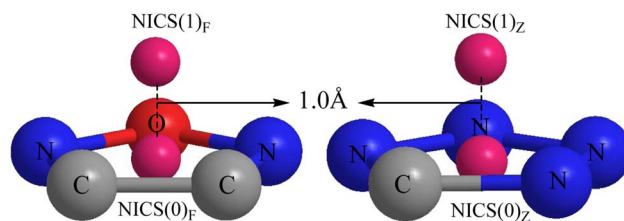


Fig. 1 Schematic of  $\lambda_{\text{NICS}(0)\text{F}}$  and  $\lambda_{\text{NICS}(0)\text{Z}}$  calculated at the center of the plane and  $\lambda_{\text{NICS}(1)\text{F}}$  and  $\lambda_{\text{NICS}(1)\text{Z}}$  calculated at 1.0 Å out of the plane.  $\lambda_{\text{NICS}(0)\text{F}}$  and  $\lambda_{\text{NICS}(1)\text{F}}$  are the indexes of aromaticity in the furazan (furoxan) ring, while  $\lambda_{\text{NICS}(0)\text{Z}}$  and  $\lambda_{\text{NICS}(1)\text{Z}}$  are the indexes of aromaticity in the tetrazole ring.

calculated at 1.0 Å away from the mass center of the corresponding plane, and these terms describe the  $\pi$  aromaticity. A graphical representation of  $\lambda_{\text{NICS}(0)\text{F}}$ ,  $\lambda_{\text{NICS}(0)\text{Z}}$  calculated at the center of the plane and  $\lambda_{\text{NICS}(1)\text{F}}$ ,  $\lambda_{\text{NICS}(1)\text{Z}}$  calculated at 1.0 Å out of the plane is shown in Fig. 1. The Multiwfn software program<sup>73</sup> was used to measure the center of mass of the furazan (furoxan) and tetrazole rings.

$\Delta V$  is the difference between  $V_{\text{eff}}$  and  $V_{\text{int}}$ , as shown in eqn (1).  $V_{\text{eff}}$  is the effective volume of a molecule that completely fills the unit cell and  $V_{\text{int}}$  is the intrinsic gas-phase molecular volume.  $\Delta V$  is an important descriptor because the availability of more space indicates that a molecule has a stronger ability to absorb and localize, vibrationally or translationally.<sup>74,75</sup>

$$\Delta V = V_{\text{eff}} - V_{\text{int}} \quad (1)$$

The 0.003 au contour has been reported to provide a range of packing coefficients and also an average value, both of which are very close to the crystallographic data.<sup>75</sup>

Electrostatic potential (ESP) has significant fundamental significance and is commonly used to analyze and predict noncovalent interactions. The total variance of the electrostatic potential value on the van der Waals molecular surface ( $\sigma_{\text{tot}}^2$ ), positive electrostatic potential variance ( $\sigma_+^2$ ), and negative electrostatic potential variance ( $\sigma_-^2$ ) are the means of statistically-defined quantities. These three indexes are usually used to characterize the surface potential.<sup>74</sup> Among them,  $\sigma_{\text{tot}}^2$  is the sum of  $\sigma_+^2$  and  $\sigma_-^2$ , which are defined as followed.

$$\sigma_{\text{tot}}^2 = \sigma_+^2 + \sigma_-^2 \quad (2)$$

$$\sigma_+^2 = \frac{1}{m} \sum_{i=1}^m [V_s^+(r_i) - \bar{V}_s^+]^2 \quad (3)$$

$$\sigma_-^2 = \frac{1}{n} \sum_{j=1}^n [V_s^-(r_j) - \bar{V}_s^-]^2 \quad (4)$$

$$V(r) = \sum_A \frac{Z_A}{|R_A - r|} - \int \frac{\rho(r') dr'}{|r' - r|} \quad (5)$$

where  $V_s^+(r_i)$  is the positive value of  $V(r)$ ,  $V_s^-(r_j)$  is the negative value of  $V(r)$ ,  $\bar{V}_s^+$  is the average of the positive ESPs, and  $\bar{V}_s^-$  is the average of the negative ESPs on the molecular surface. Eqn (5) can be used to calculate the electrostatic potential at any



point  $r$ , where  $Z_A$  is the charge on nucleus A, located at  $R_A$ , and  $\rho(r')$  is the electronic density.

$I$  and  $A$  can be obtained *via* the calculations based on the energy difference of neutral and anionic or cationic species<sup>76</sup>

$$I = E_{\text{cation}} - E_{\text{neutral}} \quad (6)$$

$$A = E_{\text{neutral}} - E_{\text{anion}} \quad (7)$$

where  $E_{\text{cation}}$  is the cation energy,  $E_{\text{anion}}$  is the anion energy, and  $E_{\text{neutral}}$  is the neutral compound energy.

Bond order was first proposed by Pauling<sup>77</sup> and can be used to characterize bond strength. A larger bond order value indicates a stronger chemical bond, while a smaller bond order indicates a weaker bond, which is easier to break up. Bond order is commonly represented by the phenomenological bond order and theoretical bond order.<sup>78</sup> Determining the phenomenological bond order requires bond lengths and symmetrical stretching frequencies, which are experimentally measured. The theoretical bond order is unobservable and has no unique definition or physical basis.<sup>79</sup> The WBO is a commonly used definition of theoretical bond order.<sup>80</sup> Therefore, the weakest chemical bond can be found by calculating the WBO. A small value of WBO indicates a weak bond, which may work as a trigger bond.<sup>81</sup> Since the breaking of the weakest chemical bond in energetic materials may lead to its decomposition and affect the stability of energetic materials,<sup>82–84</sup> the WBO of the weakest chemical bond was chosen as a descriptor.<sup>85,86</sup>

Meanwhile, in order to generate a relatively reliable simulation result, additional simulations with different sets of descriptors (7, 8, 9, 10, 11, 12 and 13 descriptors) were performed, and their results are summarized in Table S1 (ESI).† RMSE presents a fluctuating downward tendency with the increase in the number of descriptors and reached the smallest value with 13 descriptors. However, the  $R^2$  does not present a simple linear dependence on the number of descriptors and reaches the largest value in the case 13 descriptors. As can be seen, the models with smallest number of descriptors, 7 or 8, perform poorly. In particular, the RMSE of 64.42 and  $R^2$  of 50.89% are obtained in the case of 8 descriptors. This indicates that these models failed to capture the necessary information about the molecular structure, which leads to underfitting, where the models were too simple to fully learn the underlying patterns. In order to comprehensively describe the key molecular structural features, the model with 13 descriptors was selected. These descriptors include most valuable information relevant directly on the stability and reactivity. However, since the largest descriptors (13) combined with a small dataset may lead to overfitting, dimensionality reduction techniques and cross-validation were employed to optimize the model. The correlation coefficients between each descriptor and  $T_d$  are shown in Table S2,† with WBO, OB,  $A_{\text{NICS}(0)\text{F}}$  and  $A_{\text{NICS}(0)\text{Z}}$  being the most relevant to  $T_d$  prediction.

## 2.2 Quantitative structure–property relationships

A nonlinear QSPR model was employed to study the relationship between the  $T_d$  values and structures of nitrogen-rich

energetic ionic salts. This model was developed by SVM approach with radial basis function (RBF) as the kernel function.<sup>87</sup> The purpose of the kernel function is to map objects to a feature space, and RBF is one of the more commonly used kernel functions.<sup>88</sup> Because the RBF kernel is nonlinear, the built QSPR model is also nonlinear.

PCA<sup>89</sup> was used for dimensional reduction. The principle of PCA involves the formation of a latent variable through the linear combination of original variables, which allows for the generation of new orthogonal axes to rationalize the maximum possible variance in only a few dimensions. Then, the QSPR of the  $T_d$  values and descriptors processed in the reduced dimensions was built by SVM, which was freely available in the LIBSVM software.<sup>90</sup> MATLAB 2013a was used to perform all simulations.

## 3. Discussion

### 3.1 Sample analysis

The selection of experimental data is an important part of QSPR studies because experimental conditions may have a strong effect on the studied target property. Thus, it is necessary to ensure that all experimental values were measured under the same conditions. In this study, 21 nitrogen-rich energetic ionic salts were chosen. These ionic salts were measured under the same conditions by the same research group,<sup>3–5</sup> and their structures and  $T_d$  values are shown in Table 1.

The optimized geometries of the 21 nitrogen-rich energetic ionic salts at the M06-2X/6-311++G(3df,3pd) level of theory are shown in Fig. S1 (ESI).† The number (No.) of each energetic ionic salt is referenced in Table 1. All the anions of these nitrogen-rich energetic ionic salts have two common aromatic rings: a furazan (furoxan) ring and a tetrazole ring. These anions are paired with nitrogen-rich cations such as ammonium, hydrazinium, guanidinium, and azolium. As shown in Table 1, the nitrogen-rich energetic ionic salts based on bis-heterocycle-substituted 1,2,3-triazole (HTANFT) and 3,4-bis(1H-5-tetrazolyl)furoxan ( $H_2$ BTF) all have  $T_d$  values higher than 200 °C except for No. 11. These  $T_d$  values are comparable to that of the traditional explosive 1,3,5-trinitro-1,3,5-triazinane (RDX;  $T_d = 230$  °C),<sup>3</sup> suggesting that HTANFT and  $H_2$ BTF show excellent promise for the design of thermally stable energetic ionic salts. In contrast, the nitrogen-rich energetic ionic salts based on 4-nitro-3-(5-tetrazole)-furoxan (HTNF) show relatively low  $T_d$  values. Among them, the *N*-carbamoylguanidinium salt (No. 7) has the highest  $T_d$ , indicating that *N*-carbamoylguanidinium shows good potential as the cation of thermally stable energetic ionic salts.

### 3.2 Local reactivity

The frontier molecular orbitals (HOMO and LUMO) are closely related to chemical reactions.<sup>60,61</sup> Therefore, to investigate the reactivity of energetic ionic salts, the HOMO and LUMO distributions must be known. As shown in Fig. 2(a), the HOMO and LUMO of the 21 nitrogen-rich energetic ionic salts are mainly located in their anions, indicating that the anions are the main



**Table 1** Structures and thermal decomposition temperatures  $T_d$  (°C) of 21 nitrogen-rich energetic salts, where  $T_d$  were taken from ref. 3–5

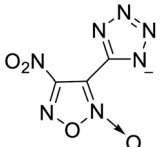
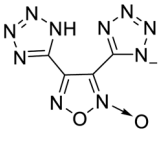
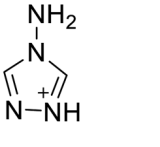
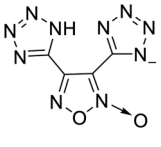
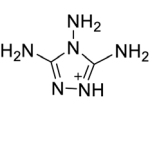
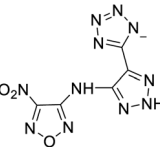
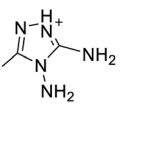
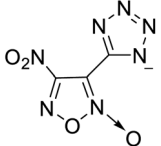
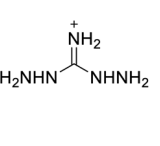
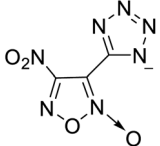
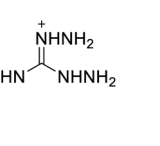
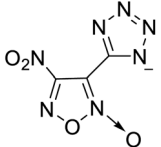
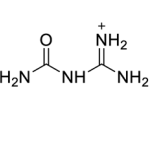
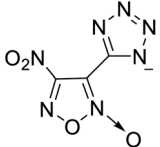
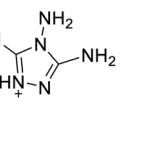
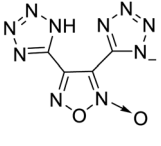
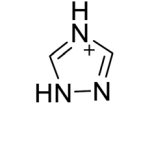
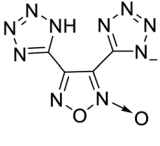
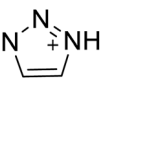
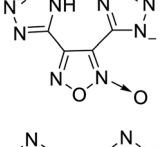
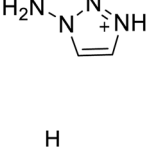
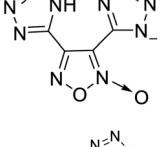
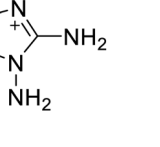
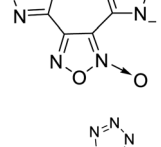
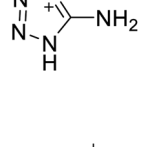
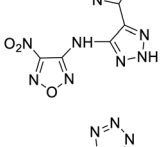
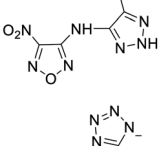
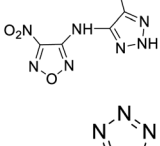
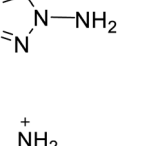
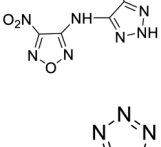
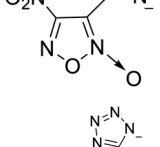
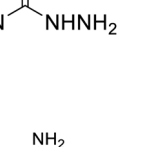
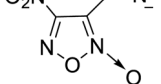
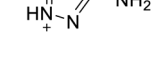
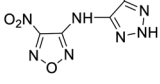
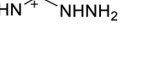
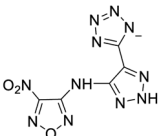
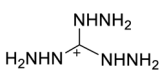
Structure				Structure			
No.	Anion	Cation	$T_d$	No.	Anion	Cation	$T_d$
1		$\text{NH}_4^+$	142	2			225
3			251	4			228
5			122	6			133
7			213	8			180
9			225	10			223
11			177	12			204
13			218	14		$\text{NH}_4^+$	224
15		$\text{H}_2\text{N}-\text{NH}_3^+$	219	16			217
17		$\text{H}_3\text{N}-\text{OH}^+$	224	18			153
19			182	20			214

Table 1 (Contd.)

No.	Structure			$T_d$	No.	Structure			$T_d$
	Anion	Cation				Anion	Cation		
21				187					

active region. Furthermore, the decomposition process of energetic materials is significantly influenced by the breaking of the weakest chemical bond.<sup>91,92</sup> For example, the weakest C–N bond dissociation of nitro compounds is considered to be the rate-determining step of their decomposition process.<sup>91</sup> The WBO of each salt is shown in Fig. 2(b). As can be seen, the N–H bond is usually the weakest bond of these energetic ionic salts. These N–H bonds are mainly located in the frontier molecular orbital. Thus, to further evaluate the decomposition process of the studied 21 energetic ionic salts, the WBO of the weakest chemical bond of each complex was determined.

### 3.3 Descriptors calculated by quantum chemistry

In this study, M06-2X combined with the 6-311++G(3df,3pd) basis set were used to obtain the quantum chemical parameters. Some quantum chemical parameters can be expressed in different ways. For example, NICS can be calculated at different positions on atomic rings, ESP values can be calculated for different regions on molecular surfaces, and  $I$  and  $A$  can be calculated with different methods. To develop a reliable model, suitable descriptors that are strongly correlated with  $T_d$  need to be selected. In this section, the selection of these parameters will be discussed in detail. The values of these parameters are shown in Table S3,<sup>†</sup> and the absolute values of the correlation coefficients ( $|R|$ ) between these parameters and  $T_d$  are shown in Fig. 3.

**3.3.1  $A_{NICS}$ .** NICS, the negative value of the computed absolute shielding, has been widely used to characterize the aromaticity of compounds due to its simplicity and efficiency.<sup>56,93</sup> Aromaticity commonly facilitates good thermal stability.<sup>3,4,94</sup> In this study, each compound contains at least two aromatic rings: a furazan (furoxan) ring and a tetrazole ring in the anion. Thus, the NICS values were calculated at the center of mass and out of the center of mass for the common furazan (furoxan) and tetrazole rings, respectively. As collected in Table S3,<sup>†</sup> all NICS values are negative, indicating that the two aromatic rings have both  $\sigma$  aromaticity and  $\pi$  aromaticity. The furazan (furoxan) ring exhibits higher  $A_{NICS(0)F}$  values compared to its  $A_{NICS(1)F}$  values, indicating that the furazan (furoxan) ring has stronger  $\sigma$  aromaticity. In contrast, the  $A_{NICS(1)Z}$  values of the tetrazole ring are higher than its  $A_{NICS(0)Z}$  values, indicating

that the tetrazole ring has stronger  $\pi$  aromaticity. To select the aromaticity descriptors for the furazan (furoxan) and tetrazole rings, the  $|R|$  values between the aromaticity descriptors and  $T_d$  were further analyzed. As shown in Fig. 3, the  $|R|$  of  $A_{NICS(0)F}$  is larger than that of  $A_{NICS(1)F}$  for the furazan (furoxan) ring ( $|R| = 0.66$  and  $0.42$ , respectively), suggesting that the  $\sigma$  aromaticity of the furazan (furoxan) ring has a more significant effect on  $T_d$ . However, the  $|R|$  of  $A_{NICS(1)Z}$  is larger than that of  $A_{NICS(0)Z}$  for the tetrazole ring ( $|R| = 0.62$  and  $0.51$ , respectively), indicating that the  $\pi$ -aromaticity of the tetrazole ring has a more important effect on  $T_d$ . As a result,  $A_{NICS(0)F}$  and  $A_{NICS(1)Z}$  were used to build the QSPR model.

**3.3.2  $\sigma_{tot}^2$ ,  $\sigma_+^2$  and  $\sigma_-^2$ .** The ESP values calculated on the van der Waals molecular surface (MSEP) can be used as descriptors to develop a reliable QSPR model for energetic materials.<sup>95</sup> The value of  $\sigma_+^2$  indicates the strength and variability of the positive surface potentials, and the value of  $\sigma_-^2$  indicates the strength and variability of the negative surface potentials. Because these terms are squared, the effects of the extrema ( $V_{s,max}$  and  $V_{s,min}$ ) are emphasized.<sup>74,96</sup> As shown in Table S3,<sup>†</sup> the ESP values on the molecular surfaces of the ionic salts show an anomalous imbalance, which may result in the breaking of the trigger bond. The positive regions are stronger and more variable than the negative regions, meaning that  $\sigma_+^2 > \sigma_-^2$ . This is because the ionic salts contain several highly electron-attracting components, such as  $-\text{NO}_2$  and aza-nitrogen atoms. Thus, the surface potential above the central portion of each compound is likely to be strongly positive, while the periphery is mainly negative.<sup>74</sup> The  $|R|$  values between  $\sigma^2$  and  $T_d$  are shown in Fig. 3. The  $|R|$  values of  $\sigma_+^2$  are higher than those of  $\sigma_{tot}^2$  and  $\sigma_-^2$ . Therefore,  $\sigma_+^2$  was employed as a descriptor to develop the QSPR model.

**3.3.3  $I$  and  $A$ .**  $I$  reflects the ability of a molecule to donate electrons and  $A$  reflects the ability of a molecule to accept electrons. A higher value of  $I$  or  $A$  indicates that a molecule has a greater ability to donate or accept electrons. In this study, these values were calculated using two methods: (i) the vertical ionization potential ( $I_v$ ) can be expressed as  $I_v = E_M^+ - E_M$ , where  $E_M$  is the energy of the molecule and  $E_M^+$  is the energy of the corresponding cation at the optimized neutral geometry. The vertical electron affinity ( $A_v$ ) can be expressed as  $A_v = E_M - E_M^-$ , where  $E_M$  is the energy of the molecule and  $E_M^-$  is the



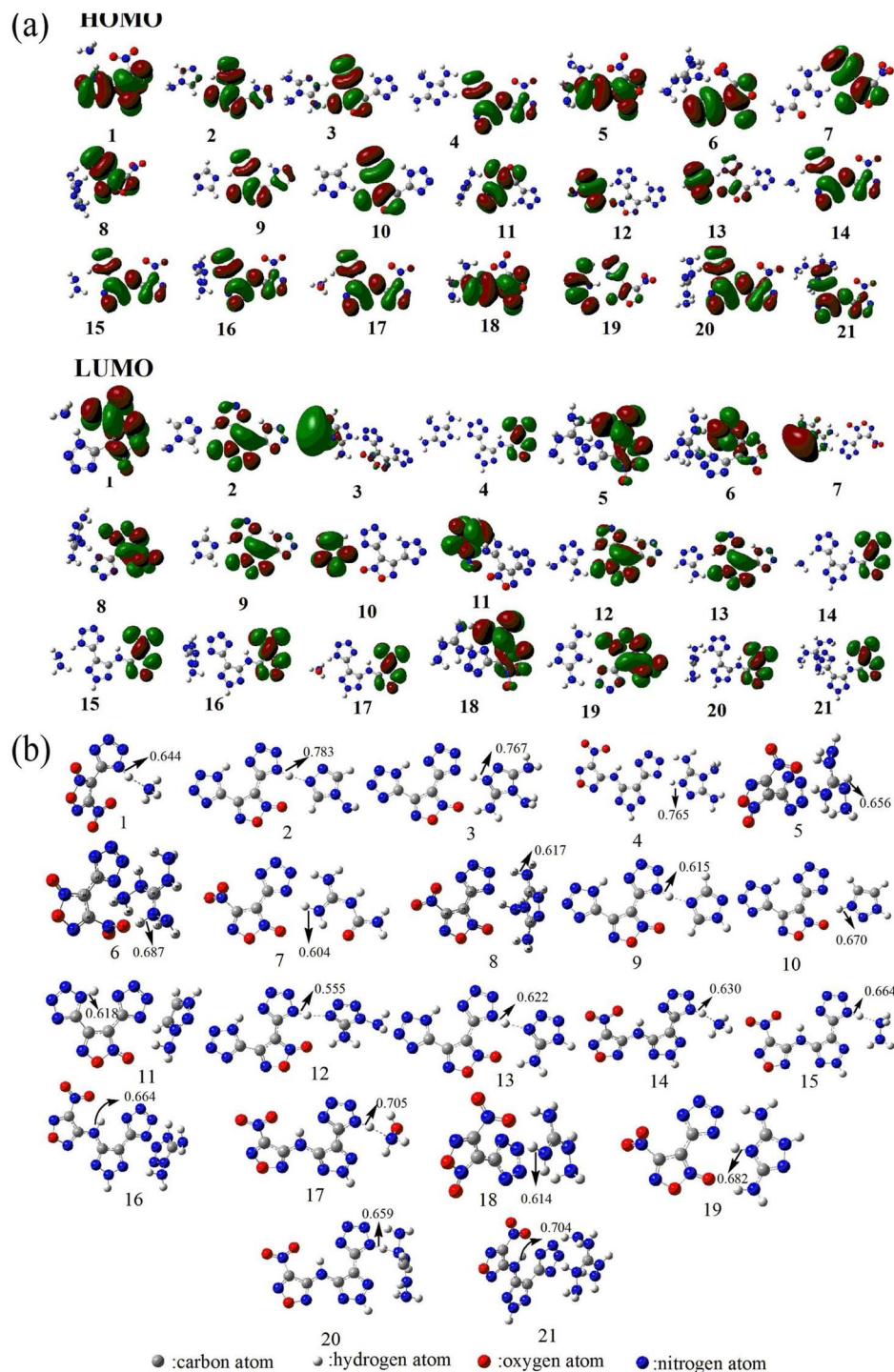


Fig. 2 (a) The highest occupied molecular orbital (HOMO) and lowest unoccupied molecular orbital (LUMO). (b) Wiberg bond order of the weakest chemical bond of the 21 nitrogen-rich energetic ionic salts at the M06-2X/6-311++G(3df,3pd) level of theory. The number of each energetic ionic salt is referenced in Table 1.

energy of the corresponding anion at the optimized neutral geometry. (ii) The adiabatic ionization potential ( $I_a$ ) and the adiabatic electron affinity ( $A_a$ ) were calculated in the same way as  $I_v$  and  $A_v$ , but the geometries of the cation and anion were optimized. Compared with  $I_v$  (or  $A_v$ ),  $I_a$  (or  $A_a$ ) considers the

relaxation of the molecular structure, and as shown in Fig. 3,  $I_a$  and  $A_a$  have higher  $|R|$  values than  $I_v$  and  $A_v$ , respectively, indicating that  $I_a$  and  $A_a$  have higher correlations with  $T_d$ . This is potentially because the thermal decomposition process is relatively slow. Therefore,  $I_a$  and  $A_a$  were employed as descriptors to

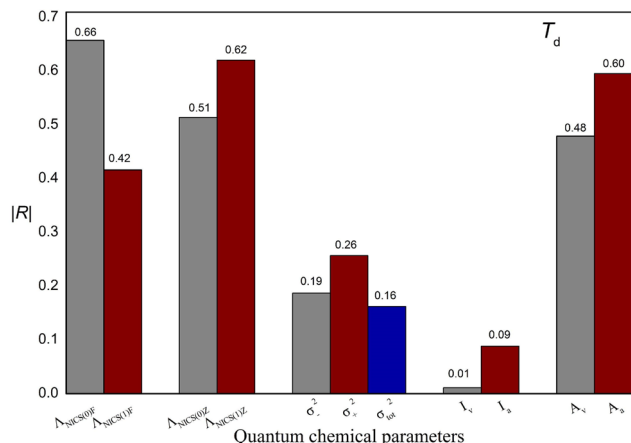


Fig. 3 Absolute values of the correlation coefficient ( $|R|$ ) between the quantum chemical parameters expressed in different ways and experimental thermal decomposition temperature ( $T_d$ ).

incorporate molecular structure relaxation into the QSPR model.

Additionally, to study the relationships between each quantum chemical parameter and  $T_d$ , linear models were built to obtain the  $|R|$  value between each parameter and  $T_d$ . Fig. 4 shows a histogram of the  $|R|$  values of the linear models. These  $|R|$  values range from 0.06 to 0.72, indicating that the relationships between the individual parameters and  $T_d$  are not simple or direct. In other words, a single parameter is correlated with  $T_d$  but is not sufficient for predicting  $T_d$ . For instance, the WBO descriptor has the largest  $|R|$  value of 0.72. However, the values of this descriptor are not in agreement with the change in  $T_d$ . In addition, two ionic salts (No. 5 and No. 6) have the same WBO values but different  $T_d$  values, indicating that  $T_d$  is affected by multiple factors. Therefore, to better describe the relationship between these parameters and  $T_d$ , these quantum chemical parameters of the energetic ionic salts and OB were fully used to construct a reliable model.

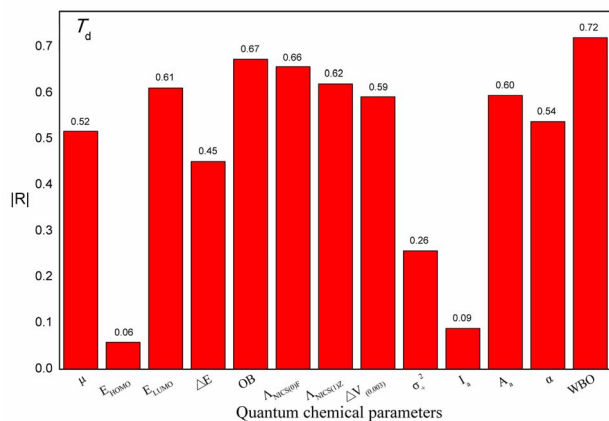


Fig. 4 Absolute values of the correlation coefficients ( $|R|$ ) between chemical parameters and experimental thermal decomposition temperature ( $T_d$ ).

### 3.4 Quantitative structure–property relationship

In this study, SVM is the ideal approach for a small number of samples<sup>79</sup> and hence used to develop a nonlinear QSPR model. All quantum chemical parameter calculations were performed under the M06-2X/6-311++G(3df,3pd) level of theory, and all the parameters were taken as descriptors (Table 2).

The main steps for constructing the QSPR model were as follows. The first step, 21 ionic salts, were divided into training set (numbers 5–21) and testing set (numbers 1–4). PCA was used to extract a descriptor data matrix from the multidimensional space to obtain a more accurate model. It should be noted that PCA does not directly remove the descriptors. Instead, PCA summarizes the information of the original data matrix and displays this information in a reduced dimensional space.<sup>97,98</sup> The procedure can be expressed as shown in Scheme 1.

$X(17 \times 13)$  is the original matrix, consisting of 13 descriptors for each of the 17 energetic ionic salts in the training set. The average value of each column from  $X$  was subtracted to obtain matrix  $A(17 \times 13)$ . The covariance matrix  $B(13 \times 13)$  was then obtained from matrix  $A$ . The latent ( $13 \times 1$ ) was obtained by arranging the eigenvalues of the covariance matrix  $B$  in descending order. The matrix  $C(13 \times 13)$  is eigenvectors, which have the same order as the eigenvalues in the latent. The eigenvalues and the proportions of matrix  $C$  described by the first four components are shown in Table 3. These four components can contain 99.99% of the total information of the energetic ionic salts. Next, the first four volumes of matrix  $C$  were extracted to form matrix  $D(13 \times 4)$ . Matrix  $D$  was multiplied by the training set matrix ( $17 \times 13$ ) to obtain matrix  $E(17 \times 4)$ . Additionally, matrix  $D$  was multiplied by the testing set matrix ( $4 \times 13$ ) to obtain matrix  $F(4 \times 4)$ . Thus, the dimension reduction of the descriptor matrix was achieved. Finally, matrix  $E$ , matrix  $F$ , and the four important components were used to develop the nonlinear QSPR. All the matrices and latent are reported in the ESI.†

As shown in Table 3, the proportion described by the first principal component is 98.05%, which means that the first principal component can explain 98.05% of the total information. However, the specific relationship between the first principal component and the descriptors of the energetic ionic salts is uncertain. This is because the first principal component was obtained by transforming the original data matrix.

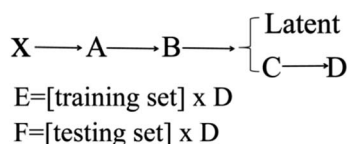
The second step for constructing the QSPR model was the optimization of SVM parameters. The selection of the kernel function parameters is crucial for SVM regression performance. In this study, the most important parameters for the SVM model are the regularization parameter  $c$  and the kernel parameter  $g$ . The value of  $c$  controls the trade-off between maximizing the margin and minimizing the training error, while the value of  $g$  determines the generalization ability of the SVM approach. Therefore, it is necessary to find the global optimal values of  $c$  and  $g$ . The global optimal values of  $c$  and  $g$  were evaluated by applying the “leave-one-out cross-validation” method to the training set data. The global optimal values of  $c$  and  $g$  were respectively determined to be 0.93 and 0.35 when the minimum mean square error value was obtained by “leave-one-out cross-



**Table 2** Quantum chemical descriptors and OB values of the nitrogen-rich energetic salts at the M06-2X/6-311++G(3df,3pd) level of theory. The number is referenced in Table 1<sup>a</sup>

No.	$\mu$ /Debye	$E_{\text{HOMO}}$ /eV	$E_{\text{LUMO}}$ /eV	$\Delta E$ /eV	OB	$A_{\text{NICS}(0)\text{F}}$	$A_{\text{NICS}(1)\text{Z}}$	$\Delta V_{(0.003)}/\text{\AA}^3$	$\sigma_+^2/(\text{kcal mol}^{-1})^2$	$I_a$ /eV	$A_a$ /eV	$\alpha/\text{Bohr}^3$	WBO
1	6.25	-9.16	-2.77	-6.39	-29.6	-13.33	-13.35	53.04	221.08	8.98	2.63	116.30	0.64
2	13.62	-9.16	-1.88	-7.28	-67.9	-10.95	-13.23	75.94	293.53	8.88	1.78	179.84	0.62
3	20.37	-8.49	-1.46	-7.03	-66.6	-11.26	-13.92	82.04	495.31	8.45	1.82	201.92	0.56
4	18.36	-7.38	-1.61	-5.77	-65.4	-12.32	-13.22	92.30	489.94	7.68	1.86	228.61	0.61
5	6.81	-8.37	-2.46	-5.91	-44.4	-13.34	-14.73	65.55	234.41	8.48	2.70	158.41	0.77
6	11.49	-8.05	-2.39	-5.66	-44.8	-13.78	-14.31	69.40	259.24	8.24	2.67	167.70	0.77
7	16.61	-8.17	-1.46	-6.70	-45.1	-13.70	-14.16	72.86	614.82	8.30	1.46	168.05	0.66
8	10.74	-8.35	-1.64	-6.72	-48.5	-13.81	-14.05	72.48	415.25	8.35	1.93	172.70	0.69
9	9.25	-9.37	-2.07	-7.30	-68.7	-11.11	-13.15	71.61	240.87	9.17	1.95	168.94	0.62
10	18.89	-8.47	-1.83	-6.64	-68.7	-11.38	-13.88	70.24	651.07	8.55	1.68	171.40	0.61
11	17.48	-8.26	-1.72	-6.54	-67.9	-11.29	-14.48	72.97	656.95	8.41	1.78	176.84	0.67
12	11.49	-9.25	-2.13	-7.11	-54.6	-11.10	-13.23	77.50	254.36	9.41	2.14	185.74	0.62
13	10.74	-9.43	-2.21	-7.22	-54.7	-11.18	-13.17	73.53	350.53	9.23	2.21	175.38	0.63
14	10.05	-8.33	-2.10	-6.23	-56.7	-12.13	-12.63	69.78	237.42	8.70	1.83	163.81	0.66
15	10.26	-8.33	-2.10	-6.23	-56.5	-12.13	-12.64	73.95	253.29	8.74	1.84	172.84	0.66
16	13.26	-7.62	-1.77	-5.84	-54.7	-12.26	-13.75	84.30	436.67	7.81	2.98	207.73	0.70
17	8.35	-8.43	-2.17	-6.26	-48.3	-12.10	-12.48	72.25	264.09	8.75	1.89	167.87	0.68
18	7.69	-8.32	-2.47	-5.85	-43.9	-13.33	-14.96	62.58	338.45	8.47	2.66	149.79	0.78
19	10.41	-8.41	-1.74	-6.67	-48.3	-13.89	-14.19	70.14	369.49	7.77	2.23	167.02	0.60
20	9.26	-8.41	-2.16	-6.25	-63.2	-12.21	-12.68	85.32	249.80	7.95	2.44	206.10	0.66
21	7.67	-7.80	-2.13	-5.66	-62.8	-12.18	-14.14	86.80	320.33	7.84	2.91	213.89	0.70

<sup>a</sup>  $\mu$ /Debye: dipole moment  $E_{\text{HOMO}}$ /eV: energy of the highest occupied molecular orbital  $E_{\text{LUMO}}$ /eV: energy of the lowest unoccupied molecular orbital  $\Delta E$ : energy gap between the HOMO and LUMO OB: oxygen balance  $A_{\text{NICS}(0)\text{F}}$ : index of aromaticity calculated at the central of the furazan (furoxan)  $A_{\text{NICS}(1)\text{Z}}$ : index of aromaticity calculated at 1.0 Å out of the tetrazole  $\Delta V_{(0.003)}/\text{\AA}^3$ : available free space per molecule in the unit cell  $\sigma_+^2/(\text{kcal mol}^{-1})^2$ : positive ESP variance  $I_a$ /eV: adiabatic ionization potential  $A_a$ /eV: adiabatic electron affinity  $\alpha/\text{bohr}^3$ : polarizability WBO: Wiberg bond order of the weakest chemical bond.



**Scheme 1** The main dimension reduction process of the model construction for 21 nitrogen-rich energetic ion salts with 13 descriptor data.

**Table 3** The eigenvalues and proportion of variance explained by the first four components using the covariance matrix

Component	Eigenvalue	Proportion (%)	Accumulation (%)
1	21762.47	98.05	98.05
2	371.19	1.67	99.73
3	55.51	0.25	99.98
4	2.83	0.01	99.99

validation". Additionally, leave- $p$ -out<sup>99</sup> and  $k$ -fold cross-validation<sup>100</sup> are also suitable for the QSPR studies of the small sample data to provide a robust model performance and generalize well to the unseen data.

The final step for constructing the QSPR model is to evaluate the model. The root-mean-square error (RMSE) and correlation coefficient ( $R^2$ ) values were used to evaluate the performance of

the model. The values of RMSE<sup>101</sup> and  $R^2$  (ref. 102) were calculated with the following equations.

$$\text{RMSE} = \sqrt{\frac{\sum_{i=1}^n (x_i - y_i)^2}{n}} \quad (8)$$

$$R^2 = \frac{\left( n \sum_{i=1}^n x_i y_i - \sum_{i=1}^n x_i \sum_{i=1}^n y_i \right)^2}{\left( n \sum_{i=1}^n x_i^2 - \left( \sum_{i=1}^n x_i \right)^2 \right) \left( n \sum_{i=1}^n y_i^2 - \left( \sum_{i=1}^n y_i \right)^2 \right)} \quad (9)$$

where  $y_i$  is the experimental  $T_d$  value,  $x_i$  is the predicted experimental  $T_d$  value, and  $n$  is the number of samples. Table 4 collects the  $T_d$  values of the training and testing sets predicted using the constructed model. The comparison between the experimental and predicted  $T_d$  for 21 energetic ionic salts is shown in Fig. 5. As can be seen, the RMSE of the testing set, which means the differences between predicted and experimental  $T_d$ , was 15.72, and the  $R^2$  was 96.31%. For further comparison, MLR and LASSO regression model simulations were performed to study the relationship between  $T_d$  and descriptors. The RMSE and  $R^2$  of the MLR model were 22.77 and 77.06%, the RMSE and  $R^2$  of the LASSO model were 16.75 and 83.61%, respectively. This means that the nonlinear correlation model used in this study has stronger fitting ability and provides higher predictivity compared to the linear correlation model and also indicates the adequate performance of the developed model. Therefore, although linear models have



**Table 4** The experimental (exp) and predicted (pred) thermal decomposition temperatures ( $T_d$ ) of the training set and testing set. The number of each energetic salt is referenced in Table 1

No.	Exp <sup>a</sup>	Pred	Residue	Number	Exp <sup>a</sup>	Pred	Residue
1 <sup>c</sup>	142	161	−19	12 <sup>b</sup>	204	221	−17
2 <sup>c</sup>	225	243	−18	13 <sup>b</sup>	218	206	12
3 <sup>c</sup>	251	247	4	14 <sup>b</sup>	224	217	7
4 <sup>c</sup>	228	242	−14	15 <sup>b</sup>	219	218	1
5 <sup>b</sup>	122	161	−39	16 <sup>b</sup>	217	212	5
6 <sup>b</sup>	133	198	−65	17 <sup>b</sup>	224	194	30
7 <sup>b</sup>	213	212	1	18 <sup>b</sup>	153	152	1
8 <sup>b</sup>	180	183	−3	19 <sup>b</sup>	182	183	−1
9 <sup>b</sup>	225	224	1	20 <sup>b</sup>	214	215	−1
10 <sup>b</sup>	223	222	1	21 <sup>b</sup>	187	188	−1
11 <sup>b</sup>	177	211	−34				

<sup>a</sup> Thermal decomposition temperatures were taken from ref. 3–5. <sup>b</sup> The molecules in the training set. <sup>c</sup> The molecules in the testing set.

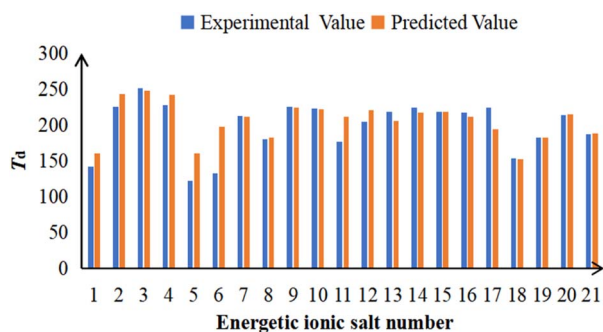


**Fig. 5** The comparison between the experimental and predicted  $T_d$  for 21 energetic ionic salts. The number of energetic ionic salt is referenced in Table 1.

advantages over nonlinear ones such as high computational efficiency and strong interpretability of results, their ability to fit nonlinear relationship data such as the relationship between the  $T_d$  of ionic salts and descriptors is poor. Nonlinear models, while powerful in capturing complex relationships between descriptors and  $T_d$ , can become overly sensitive to the specific patterns in the training data. To mitigate this, cross-validation was employed to monitor the performance of the developed models; however, the relatively high RMSE indicates that further refinement may be required to ensure that the model does not overfit the training set and retains its generalizability in the case of other compounds. At the same time, we noticed significant differences between the experimental and the predicted values of energetic ionic salts 5 and 6, which may be due to the lower  $T_d$  of these two molecules, while the  $T_d$  of other selected samples were much higher (averaging about 200 °C). The reason why energetic ionic salts 5 and 6 were ultimately retained as the sample data is that the synthesis process of the energetic ionic salts is complex and there are few available samples. If samples with a wider range of  $T_d$  values can be synthesized in the future, we will further investigate more similar QSPR models simulations.

### 3.5 The potential limitations of the model

Except for the leave-one-out cross-validation with the  $R^2$  of 96.31% and RMSE of 15.72, which indicates the reliability of the developed QSPR model,  $k$ -fold cross-validation ( $k = 8$  and 10) were performed in order to ensure the predictive power of our model. At  $k = 8$ , the RMSE and  $R^2$  are 16.38 and 93.87%, respectively. At  $k = 10$ , the RMSE and  $R^2$  are 15.82 and 96.03%, respectively, also indicating that the developed QSPR model is quite reliable. Moreover, the reliability of the QSPR model verified by leave-one-out cross-validation is relatively higher than that of  $k$ -fold cross validation for the small dataset of energetic ionic salts considered in the present study. Due to the difficulty in preparing energetic ionic salts and measuring their  $T_d$ , the number of similar ionic salts prepared and measured at the same experiment conditions was limited. Hence, only 21 samples were selected in this study to maintain the accuracy and consistency of the samples. The relatively small dataset may raise a potential risk of overfitting, where the model may perform well on the training set but poorly on new data. Hence, cross-validation techniques, such as leave-one-out cross-validation and  $k$ -fold cross-validation, were employed to mitigate this risk. However, the limited dataset size may still be an issue in the case of the model application to a broader set of data. Moreover, the lack of validation on a broader set of compounds, including those outside the class of nitrogen-rich energetic ionic salts, may affect the conclusions about the applicability of this model to other materials and larger datasets. Further research is needed in order to evaluate the model performance on different energetic materials and larger data sets.

### 3.6 Nitrogen-rich energetic ionic salts design and prediction

Based on the analysis of the structural characteristics of the nitrogen-rich energetic ionic salts with relatively high  $T_d$  values, 6 new energetic ionic salts were further designed. The anions of these salts are based on HTANFT or  $H_2BTF$ . Among the energetic ionic salts based on  $H_2BTF$ , ionic salt No. 10 shows a relatively high  $T_d$ , indicating that ionic salts prepared with 1H-1,2,3-triazolium as the cation may exhibit high  $T_d$  values. Among the energetic ionic salts based on HTNF, ionic salt No. 7 has the highest  $T_d$ , indicating that  $N$ -carbamoylguanidinium may be an excellent functional group. In addition, the salts containing aminoguanidinium derivatives as the cation (such as No. 5 and No. 20) have different  $T_d$  values. This shows that the derivatives of aminoguanidinium can be potentially used for the design of thermally stable energetic ionic salts paired with suitable anions. As a result, the designed nitrogen-rich energetic ionic salts with anions based on HTANFT were paired with 1H-1,2,3-triazolium, 5-amino-tetrazolium, and  $N$ -carbamoylguanidinium. The nitrogen-rich energetic ionic salts based on  $H_2BTF$  were paired with aminoguanidinium, diamino-guanidinium, and triaminoguanidinium.

The 6 designed energetic ionic salts were optimized at the M06-2X/6-311++G(3df,3pd) level of theory, and all descriptors are collected in Table S4† to predict  $T_d$ . As shown in Table 5, the predicted  $T_d$  values of these new nitrogen-rich energetic ionic



**Table 5** Molecular structures and predicted thermal decomposition temperatures  $T_d$  (°C) of 6 designed theoretically designed nitrogen-rich energetic salts

Structure				Structure			
No.	Anion	Cation	$T_d$	No.	Anion	Cation	$T_d$
1			221	2			225
3			194	4			217
5			220	6			215

salts are relatively high, ranging from 194 to 225 °C. These  $T_d$  values are higher than that of 4-amino-3,5-dinitro-1H-pyrazole (LLM-116:178 °C) and Nos. 1, 2 and 5 are comparable to that of the RDX (230 °C), indicating that the designed energetic ionic salts show good promise for the preparation of thermally stable energetic materials, which may be used in special materials such as rockets, spacecraft, and devices for high-altitude aircraft in the future.

## 4. Conclusions

In this study, quantitative structure–property relationship (QSPR) model of the  $T_d$  of nitrogen-rich energetic ionic salts was built based on the SVM approach. The  $T_d$  of 21 nitrogen-rich energetic ionic salts were firstly analyzed using the QSPR model, in which  $E_{\text{HOMO}}$ ,  $E_{\text{LUMO}}$ ,  $\Delta E$ ,  $\mu$ ,  $\alpha$ , OB,  $A_{\text{NICS}(0)\text{F}}$ ,  $A_{\text{NICS}(1)\text{Z}}$ ,  $\Delta V$ ,  $\sigma^2$ ,  $I_a$ ,  $A_a$ , and WBO of the weakest chemical bond were comprehensively taken as descriptors. Also, all the descriptors were chosen by PCA for dimensional reduction. The correlation coefficient ( $R^2$ ) of the testing set is 96.31%, and the root-mean-square error (RMSE) of the testing set is 15.72 for the built QSPR model, indicating a reliable performance. Furthermore, 6 new energetic ionic salts were designed, and their  $T_d$  were predicted with the built QSPR model. The predicted  $T_d$  ranged from 194 to 225 °C, which are better than LLM-116 (178 °C), and the designed No. 1, 2 and 5 are similar to that of RDX (230 °C), indicating the excellent potential of these designed energetic ionic salts.

The optimized QSPR model has been used to predict the  $T_d$  of nitrogen-rich energetic ionic salts and has shown good predictive ability. It could provide effective method support for

the design and preparation of energetic materials where laboratory synthesis research is usually costly, time-consuming, expensive and dangerous to quickly and effectively obtain stable explosive materials. Due to the diverse and complex structures of energetic ionic salt explosives, this model has the potential to be applied in further predicting the thermodynamic characteristics of different types of energetic ionic salts and guiding the development of related experimental research. It would be fair to admit that despite applying dimensionality reduction techniques, such as PCA, and cross-validation to optimize the model, there still exists the possibility of over-fitting. Further research is needed to address this issue by expanding the dataset and by exploring simpler models that may offer a better balance between the model complexity and its generalizability.

## Data availability

The data supporting this article have been included as part of the ESI.†

## Conflicts of interest

The authors declare that they have no conflict of interest.

## Acknowledgements

The authors thank the National Natural Science Foundation of China (No. 22306179) for support of this research.



## References

- G. Fayet, P. Rotureau, L. Joubert, *et al.*, Predicting Explosibility Properties of Chemicals from Quantitative Structure-Property Relationships, *Process Saf. Prog.*, 2010, **29**, 359–371.
- G. Fayet, P. Rotureau, L. Joubert, *et al.*, On the prediction of thermal stability of nitroaromatic compounds using quantum chemical calculations, *J. Hazard. Mater.*, 2009, **171**, 845–850.
- H. Huang, Z. Zhou, L. Liang, *et al.*, Nitrogen-Rich Energetic Monoanionic Salts of 3,4-Bis(1H-5-tetrazolyl)furoxan, *Chem.-Asian J.*, 2012, **7**, 707–714.
- C. Bian, K. Wang, L. Liang, *et al.*, Nitrogen-Rich Energetic Salts of Bis-Heterocycle-Substituted 1,2,3-Triazole (HTANFT), *Eur. J. Inorg. Chem.*, 2014, **35**, 6022–6030.
- L. Liang, K. Wang, C. Bian, *et al.*, 4-Nitro-3-(5-tetrazole)furoxan and Its Salts: Synthesis, Characterization, and Energetic Properties, *Chem.-Eur. J.*, 2013, **19**, 14902–14910.
- J. Song, K. Wang, L. Liang, *et al.*, High-energy-density materials based on 1-nitramino-2,4-dinitroimidazole, *RSC Adv.*, 2013, **3**, 10859–10866.
- V. Thottampudi, J. Zhang, C. He, *et al.*, Azo substituted 1,2,4-oxadiazoles as insensitive energetic materials, *RSC Adv.*, 2014, **4**, 50361–50364.
- D. Fischer, T. M. Klapötke and J. Stierstorfer, 1,5-Di(nitramino)tetrazole: High Sensitivity and Superior Explosive Performance, *Angew. Chem., Int. Ed.*, 2015, **54**, 10299–10302.
- Y. Shao, W. Zhu and H. Xiao, Structure-property relationships of energetic nitrogen-rich salts composed of triaminoguanidinium or ammonium cation and tetrazole-based anions, *J. Mol. Graph. Model.*, 2013, **40**, 54–63.
- A. K. Sikder and N. Sikder, A review of advanced high performance, insensitive and thermally stable energetic materials emerging for military and space applications, *J. Hazard. Mater.*, 2004, **112**, 1–15.
- M. J. Kamlet and H. G. Adolph, The relationship of impact sensitivity with structure of organic high explosives II. Polynitroaromatic explosives, *Propellants, Explos. Pyrotech.*, 1979, **4**, 30–34.
- F. Luan, H. Liu, Y. Wen, *et al.*, QSPR Study for Estimation of Density of Some Aromatic Explosives by Multiple Linear Regression Approach, *Propellants, Explos. Pyrotech.*, 2010, **35**, 169–174.
- A. K. Chew, M. Sender, Z. Kaplan, *et al.*, Advancing material property prediction: using physics-informed machine learning models for viscosity, *J. Cheminf.*, 2024, **16**(1), 31.
- F. Cravero, M. F. Diaz and I. Ponzoni, Polymer informatics for QSPR prediction of tensile mechanical Properties case study: Strength at break, *J. Chem. Phys.*, 2022, **156**, 204903.
- H. Zheng, W. Lv, Y. Wang, *et al.*, Molecular kinematic viscosity prediction of natural ester insulating oil based on sparse Machine learning models, *J. Mol. Liq.*, 2023, **385**, 122355.
- Q. Gou, J. Liu, H. Su, *et al.*, Exploring an accurate machine learning model to quickly estimate stability of diverse energetic materials, *Isience*, 2024, **27**(4), 1–18.
- J. Feng, Z. Dong, Y. Ji, *et al.*, Accelerating the Discovery of Metastable IrO<sub>2</sub> for the Oxygen Evolution Reaction by the Self-Learning-Input Graph Neural Network, *JACS Au*, 2023, **3**(4), 1131–1140.
- J. Burés and I. Larrosa, Organic reaction mechanism classification using machine learning, *Nature*, 2023, **613**, 689–695.
- J. Li, A multivariate relationship for the impact sensitivities of energetic N-nitrocompounds based on bond dissociation energy, *J. Hazard. Mater.*, 2010, **174**, 728–733.
- N. R. Badders, C. Wei, A. A. Aldeeb, *et al.*, Predicting the impact sensitivities of polynitro compounds using quantum chemical descriptors, *J. Energ. Mater.*, 2006, **24**, 17–33.
- V. Prana, G. Fayet, P. Rotureau, *et al.*, Development of validated QSPR models for impact sensitivity of nitroaliphatic compounds, *J. Hazard. Mater.*, 2012, **235–236**, 169–177.
- J. Xu, L. Zhu, D. Fang, *et al.*, QSPR Studies of impact sensitivity of nitro energetic compounds using three-dimensional descriptors, *J. Mol. Graph. Model.*, 2012, **36**, 10–19.
- N. Zohari, F. Abrishami and V. Zeynali, Using the QSPR approach for estimating the density of azole-based energetic compounds, *Z. Anorg. Allg. Chem.*, 2017, **643**, 2124–2137.
- M. Fathollahi and H. Sajady, Prediction of density of energetic cocrystals based on QSPR modeling using artificial neural network, *Struct. Chem.*, 2018, **29**, 1119–1128.
- N. Zohari and F. G. Mohammadkhani, Prediction of the density of energetic Cocrystals: a way to design high performance energetic materials, *Cent. Eur. J. Energ. Mater.*, 2020, **17**, 31–48.
- J. A. Morrill and E. F. C. Byrd, Development of quantitative structure property relationships for predicting the melting point of energetic materials, *J. Mol. Graph. Model.*, 2015, **62**, 190–201.
- S. Trohalaki, R. Pachter, G. W. Drake, *et al.*, Quantitative Structure-Property Relationships for Melting Points and Densities of Ionic Liquids, *Energy Fuels*, 2005, **19**, 279–284.
- A. M. Al-Fakih, Z. Y. Algarni, M. H. Lee, *et al.*, A penalized quantitative structure-property relationship study on melting point of energetic carbocyclic nitroaromatic compounds using adaptive bridge penalty, *SAR QSAR Environ. Res.*, 2018, **29**, 339–353.
- D. Wang, G. He and H. Chen, Prediction for the Detonation Velocity of the Nitrogenrich Energetic Compounds Based on Quantum Chemistry, *Russ. J. Phys. Chem. A*, 2014, **88**, 2363–2369.
- N. Zohari and F. G. Mohammadkhani, Detonation velocity assessment of energetic cocrystals using QSPR approach, *Z. Anorg. Allg. Chem.*, 2020, **646**, 30–35.



- 31 M. Fathollahi and H. Sajady, QSPR modeling of decomposition temperature of energetic cocrystals using artificial neural network, *J. Therm. Anal. Calorim.*, 2018, **133**, 1663–1672.
- 32 B. Wang, H. Yi, K. Xu, *et al.*, Prediction of the self-accelerating decomposition temperature of organic peroxides using QSPR models, *J. Therm. Anal. Calorim.*, 2017, **128**(1), 399–406.
- 33 N. Zohari, N. Sheibani and H. Z. Chavoshi, Investigation of the most effective molecular descriptors on the thermal behaviour of energetic azido-ester plasticizers through QSPR approach, *J. Therm. Anal. Calorim.*, 2018, **131**, 3157–3167.
- 34 N. Zohari, F. Abrishami and V. Zeynali, Prediction of decomposition temperature of azole-based energetic compounds in order to assess of their thermal stability, *J. Therm. Anal. Calorim.*, 2020, **141**, 1453–1463.
- 35 N. Zohari, M. H. Keshavarz and Z. Dalaei, Prediction of decomposition onset temperature and heat of decomposition of organic peroxides using simple approaches, *J. Therm. Anal. Calorim.*, 2016, **125**, 887–896.
- 36 A. Mousaviazar, Z. Shirazi, M. H. Keshavarz, *et al.*, A novel approach for prediction of exothermic decomposition temperature of energetic complexes through additive and non-additive descriptors, *J. Therm. Anal. Calorim.*, 2022, **147**, 12907–12917.
- 37 S. Lotfi, S. Ahmadi and P. Kumar, A hybrid descriptor based QSPR model to predict the thermal decomposition temperature of imidazolium ionic liquids using Monte Carlo approach, *J. Mol. Liq.*, 2021, **338**, 116465.
- 38 Z. Zhang, C. Chen, Y. Cao, *et al.*, Descriptors applicability in machine learning-assisted prediction of thermal decomposition temperatures for energetic materials: Insights from model evaluation and outlier analysis, *Thermochim. Acta*, 2024, **735**, 179717.
- 39 M. Xiao, X. Zhang, K. Xiao, *et al.*, Prediction of thermal decomposition temperatures of binary imidazolium ionic liquid mixtures using improved E-state index descriptors, *J. Loss Prev. Process.*, 2023, **84**, 105111.
- 40 V. Cherkassky and Y. Ma, Practical selection of SVM parameters and noise estimation for SVM regression, *Neural Network.*, 2004, **17**, 113–126.
- 41 L. Tang, Y. Zhou, J. Jiang, *et al.*, Radial Basis Function Network-Based Transform for a Nonlinear Support Vector Machine as Optimized by a Particle Swarm Optimization Algorithm with Application to QSAR Studies, *J. Chem. Inf. Model.*, 2007, **47**, 1438–1445.
- 42 Y. Li, Z. Dai, D. Cao, *et al.*, Chi-MIC-share: A new feature selection algorithm for quantitative structure-activity relationship models, *RSC Adv.*, 2020, **10**(34), 19852–19860.
- 43 P. Xu, X. Ji, M. Li, *et al.*, Small data machine learning in materials science, *npj Comput. Mater.*, 2023, **9**(1), 42.
- 44 T. R. Novianidy, G. M. Idroes, T. E. Tallei, *et al.*, QSAR Modeling for Predicting Beta-Secretase 1 Inhibitory Activity in Alzheimer's Disease with Support Vector Regression, *Malacca Pharm.*, 2024, **2**(2), 79–85.
- 45 M. S. Abubakar, K. O. Aremu, M. Aphane, *et al.*, A QSPR analysis of physical properties of antituberculosis drugs using neighbourhood degree-based topological indices and support vector regression, *Heliyon*, 2024, **10**(7), 1–27.
- 46 P. Hohenberg and W. Kohn, Inhomogeneous Electron Gas, *Phys. Rev.*, 1964, **136**(3B), B864–B871.
- 47 W. Kohn and L. J. Sham, Self-consistent equations including exchange and correlation effects, *Phys. Rev.*, 1965, **140**(4A), A1133–A1138.
- 48 A. J. Cohen, P. Mori-Sánchez and W. Yang, Challenges for density functional theory, *Chem. Rev.*, 2012, **112**(1), 289–320.
- 49 A. D. Becke, Perspective: Fifty years of density-functional theory in chemical physics, *J. Chem. Phys.*, 2014, **140**(18), 1–18.
- 50 K. Burke, Perspective on density functional theory, *J. Chem. Phys.*, 2012, **136**(15), 150901.
- 51 G. W. T. M. J. Frisch, H. B. Schlegel, G. E. Scuseria, *et al.*, *Gaussian 09*, Revision A.1, Gaussian, Inc., Wallingford CT, 2009.
- 52 Y. Zhao and D. G. Truhlar, The M06 suite of density functionals for main group thermochemistry, thermochemical kinetics, noncovalent interactions, excited states, and transition elements: two new functionals and systematic testing of four M06-class functionals and 12 other functionals, *Theor. Chem. Acc.*, 2008, **120**, 215–241.
- 53 E. G. Hohenstein, S. T. Chill and C. D. Sherrill, Assessment of the Performance of the M05-2X and M06-2X Exchange-Correlation Functionals for Noncovalent Interactions in Biomolecules, *J. Chem. Theory Comput.*, 2008, **4**, 1996–2000.
- 54 Y. Zhao and D. G. Truhlar, Applications and validations of the Minnesota density functionals, *Chem. Phys. Lett.*, 2011, **502**, 1–13.
- 55 S. Zhang, G. Wang, Y. Lu, *et al.*, The Interactions between Imidazolium-Based Ionic Liquids and Stable Nitroxide Radical Species: A Theoretical Study, *J. Phys. Chem. A*, 2016, **120**, 6089–6102.
- 56 J. Zhang, Q. Zhang, T. V. Thao, *et al.*, Energetic Salts with  $\pi$ -Stacking and Hydrogen-Bonding Interactions Lead the Way to Future Energetic Materials, *J. Am. Chem. Soc.*, 2015, **137**, 1697–1704.
- 57 J. Zhang, C. He, D. A. Parrish, *et al.*, Nitramines with Varying Sensitivities: Functionalized Dipyrzoyl-N-nitromethanamines as Energetic Materials, *Chem.-Eur. J.*, 2013, **19**, 8929–8936.
- 58 J. Zhang and J. M. Shreeve, Nitroaminofurazans with Azo and Azoxy Linkages: A Comparative Study Of Structural, Electronic, Physicochemical, and Energetic Properties, *J. Phys. Chem. C*, 2015, **119**, 12887–12895.
- 59 Q. Wu, W. Zhu and H. Xiao, A New Design Strategy for High-energy low-sensitivity explosives: combining oxygen balance equal to zero, a combination of nitro and amino groups, and N-oxide in one molecule of 1-Amino-5-nitrotetrazole-3N-oxide, *J. Mater. Chem. A*, 2014, **2**, 13006–13015.



- 60 M. Karelson, V. S. Lobanov and A. R. Katritzky, Quantum-Chemical Descriptors in QSAR/QSPR Studies, *Chem. Rev.*, 1996, **96**, 1027–1043.
- 61 G. Gece and S. Bilgic, Quantum chemical study of some cyclic nitrogen compounds as corrosion inhibitors of steel in NaCl media, *Corros. Sci.*, 2009, **51**, 1876–1878.
- 62 M. Tian, W. J. Chi, Q. S. Li, *et al.*, Theoretical design of highly energetic poly-nitro cage compounds, *RSC Adv.*, 2016, **6**, 47607–47615.
- 63 D. Zhai, C. Ma, P. Ma, *et al.*, Theoretical insight into different energetic groups on the performance of energetic materials featuring RDX ring, *Fuel*, 2021, **294**, 120497.
- 64 C. Li, Z. Lu, S. Li, *et al.*, The influence of the number of fluorine atoms on the properties of energetic materials, *J. Mol. Struct.*, 2024, **1318**, 139246.
- 65 X. Jin, B. Hu, W. Lu, *et al.*, Theoretical study on a novel high-energy density material 4,6,10,12-tetranitro-5,11-bis(nitroimino)-2,8-dioxo-4,6,10,12-tetraaza-tricyclo [7,3,0,03,7] dodecane, *RSC Adv.*, 2014, **4**, 6471–6477.
- 66 Z. Zhou and R. G. Parr, Activation Hardness: New Index for Describing the Orientation of Electrophilic Aromatic Substitution, *J. Am. Chem. Soc.*, 1990, **112**, 5720–5724.
- 67 G. Gece, The use of quantum chemical methods in corrosion inhibitor studies, *Corros. Sci.*, 2008, **50**, 2981–2992.
- 68 H. Zhao, X. Zhang, L. Ji, *et al.*, Quantitative structure-activity relationship model for amino acids as corrosion inhibitors based on the support vector machine and molecular design, *Corros. Sci.*, 2014, **83**, 261–271.
- 69 P. V. R. Schleyer, C. Maerker, A. Dransfeld, *et al.*, Nucleus-Independent Chemical Shifts: A Simple and Efficient Aromaticity Probe, *J. Am. Chem. Soc.*, 1996, **118**, 6317–6318.
- 70 Z. F. Chen, C. S. Wannere, C. Corminboeuf, *et al.*, Nucleus-Independent Chemical Shifts (NICS) as an Aromaticity Criterion, *Chem. Rev.*, 2005, **105**, 3842–3888.
- 71 C. Wang, X. Zhang, J. Lu, *et al.*, Theoretical studies on all-metal binuclear sandwich-like complexes  $M_2(\eta^4-E_4)_2$  ( $M=Al, Ga, In; E=Sb, Bi$ ), *J. Mol. Model.*, 2012, **18**, 3577–3586.
- 72 C. Wang, X. Zhang, M. Ge, *et al.*, The first nonmetal-centered binuclear sandwich-like complexes based on the tetraatomic species  $E_4^{2-}$  ( $E = N, P, As, Sb, Bi$ ) and boron atoms, *New J. Chem.*, 2011, **35**, 2527–2533.
- 73 T. Lu and F. Chen, Multiwfn: a multifunctional wavefunction analyzer, *J. Comput. Chem.*, 2012, **33**, 580–592.
- 74 M. Pospíšil, P. Vávra, M. C. Concha, *et al.*, A possible crystal volume factor in the impact sensitivities of some energetic compounds, *J. Mol. Model.*, 2010, **16**, 895–901.
- 75 M. Pospíšil, P. Vávra, M. C. Concha, *et al.*, Sensitivity and the available free space per molecule in the unit cell, *J. Mol. Model.*, 2011, **17**, 2569–2574.
- 76 M. G. Elghalban, A. M. E. Defarwy, R. K. Shah, *et al.*,  $\alpha$ -Furil Dioxime: DFT Exploration and its Experimental Application to the Determination of Palladium by Square Wave Voltammetry, *Int. J. Electrochem. Sci.*, 2014, **9**, 2379–2396.
- 77 L. Pauling, Atomic Radii and Interatomic Distances in Metals, *J. Am. Chem. Soc.*, 1947, **69**, 542–553.
- 78 R. F. See, Which Method of Assigning Bond Orders in Lewis Structures Best Reflects Experimental Data? An Analysis of the Octet Rule and Formal Charge Systems for Period 2 and 3 Nonmetallic Compounds, *J. Chem. Educ.*, 2009, **86**, 1241–1247.
- 79 Z. Chen and H. Xiao, Quantum Chemistry Derived Criteria for Impact Sensitivity, *Propellants, Explos. Pyrotech.*, 2014, **39**, 487–495.
- 80 K. B. Wiberg, Application of the Pople-Santry-Segal CNDO Method to Cyclopropylcarbonyl and Cyclobutyl Cation and to Bicyclobutyl, *Tetrahedron*, 1968, **24**, 1083–1096.
- 81 Y. Li, Y. Li, S. Jin, *et al.*, Molecular design of energetic tetrazine-triazole derivatives, *J. Mol. Model.*, 2021, **27**, 1–8.
- 82 S. R. Saraf, W. J. Rogers and M. S. Mannan, Application of transition state theory for thermal stability prediction, *Ind. Eng. Chem. Res.*, 2003, **42**, 1341–1346.
- 83 E. Theerlynck, D. Mathieu and P. Simonetti, Towards improved models to rationalize and estimate the decomposition temperatures of nitroalkanes, nitramines and nitric esters, *Thermochim. Acta*, 2005, **426**(1), 123–129.
- 84 Z. Yu and E. R. Bernstein, On the decomposition mechanisms of new imidazole-based energetic materials, *J. Phys. Chem. A*, 2013, **117**(8), 1756–1764.
- 85 L. Song, C. Zhang, C. Sun, *et al.*, Stabilization mechanisms of three novel full-nitrogen molecules, *Monatsh. Chem.*, 2021, **152**, 421–430.
- 86 H. Liu, P. Chen, X. Huang, *et al.*, A physical organic strategy to predict and interpret stabilities of chemical bonds in energetic compounds for the discovery of thermal-resistant properties, *J. Mol. Model.*, 2024, **30**(3), 84.
- 87 N. T. Renukadevi and P. Thangaraj, Performance Evaluation of SVM-RBF Kernel for Medical Image Classification, *J. Comput. Sci. Technol.*, 2013, **13**, 15–19.
- 88 R. Alwee, S. M. H. Shamsuddin and R. Sallehuddin, Hybrid support vector regression and autoregressive integrated moving average models improved by particle swarm optimization for property crime rates forecasting with economic indicators, *Sci. World J.*, 2013, **2013**, 11.
- 89 M. Rusu, D. Rusu and C. Sărbu, Lipophilicity of metallic complexes of 4-methoxyphenyl-4'-chlorobenzoylhydrazine as estimated from principal component analysis of thin layer chromatographic retention data, *Anal. Lett.*, 1999, **32**, 2999–3011.
- 90 E. Byvatov, U. Fechner, J. Sadowski, *et al.*, Comparison of Support Vector Machine and Artificial Neural Network Systems for Drug/Nondrug Classification, *J. Chem. Inf. Comput. Sci.*, 2003, **43**, 1882–1889.
- 91 S. R. Saraf, W. J. Rogers and M. S. Mannan, Application of transition state theory for thermal stability prediction, *Ind. Eng. Chem. Res.*, 2003, **42**, 1341–1346.
- 92 E. Theerlynck, D. Mathieu and P. Simonetti, Towards improved models to rationalize and estimate the decomposition temperatures of nitroalkanes, nitramines and nitric esters, *Thermochim. Acta*, 2005, **426**(1), 123–129.



- 93 J. Cai, C. Xie, X. Jin, *et al.*, High performance and heat-resistant pyrazole-1, 2, 4-triazole energetic materials: Tuning the thermal stability by asymmetric framework and azo-bistriazole bridge, *Chem. Eng. J.*, 2022, **433**, 134480.
- 94 X. Miao, X. Yang, Y. Li, *et al.*, Thermal stability of azole-rich energetic compounds: their structure, density, enthalpy of formation and energetic properties, *Phys. Chem. Chem. Phys.*, 2023, **25**(28), 18523–18544.
- 95 C. K. Kim, S. G. Cho, J. Li, *et al.*, QSPR Studies on Impact Sensitivities of High Energy Density Molecules, *Bull. Korean Chem. Soc.*, 2011, **32**, 4341–4346.
- 96 J. S. Murray, M. C. Concha and P. Politzer, Links between surface electrostatic potentials of energetic molecules, impact sensitivities and C-NO<sub>2</sub>/N-NO<sub>2</sub> bond dissociation energies, *Mol. Phys.*, 2009, **107**, 89–97.
- 97 C. Sârbu, T. Djaković-Sekulić, N. Perišić-Janjić, *et al.*, Evaluation of lipophilicity of some benzimidazole and benztriazole derivatives by RP HPTLC and PCA, *J. Pharm. Biomed. Anal.*, 2002, **30**, 739–745.
- 98 K. Polikreti, V. Argyropoulos, D. Charalambous, *et al.*, Tracing correlations of corrosion products and microclimate data on outdoor bronze monuments by Principal Component Analysis, *Corros. Sci.*, 2009, **51**, 2416–2422.
- 99 J. Shao, Linear model selection by cross-validation, *J. Am. Stat. Assoc.*, 1993, **88**(422), 486–494.
- 100 M. Stone, Cross-validated choice and assessment of statistical predictions, *J. R. Stat. Soc. Ser. B Methodol.*, 1974, **36**(2), 111–133.
- 101 P. Lind and T. Maltseva, Support Vector Machines for the Estimation of Aqueous Solubility, *J. Chem. Inf. Comput. Sci.*, 2003, **43**, 1855–1859.
- 102 C. C. Chang and C. J. Lin, LIBSVM: a library for support vector machines, *ACM Trans. Intell. Syst. Technol.*, 2011, **2**(3), 1–27.

